Research Article

Geometry optimization for structural reliability and performance of a thermoelectric generator

Naveen K. Karri[1] · Changki Mo[2]

Abstract
The opposing requirements for the performance and reliability of a thermoelectric generator (TEG) are investigated with numerical finite element analysis simulations. The parameters that significantly influence the operational performance and structural reliability of a TEG are considered for simultaneous optimization. The design of experiments based response surface optimization methodology in conjunction with results from finite element analysis was employed to identify optimal parameters from the structural reliability and performance (power output and efficiency) perspectives. A high temperature bismuth telluride based TEG couple was used in the studies to demonstrate the general applicability of the methodology. The response surface methodology is found to be a robust technique that can expedite the process of geometry optimization of a TE device during the research and development phase of TEG devices fabricated from novel thermoelectric materials.

Keywords Thermoelectric · Thermomechanical · Geometry · Reliability · Design of experiments · Optimization

List of symbols

A	Leg area (mm^2)
d	Leg spacing (mm)
D	Desirability
I	Electric current (mA)
L	Leg length (mm)
P	Power (W)
Pf	Probability of failure (%)
T	Absolute temperature (K)
tBar	Barrier layer thickness (mm)
tIC	Interconnect thickness (mm)
W	Leg width (mm)
Z	Figure of merit (K^{-1})
ZT	Dimensionless figure of merit

Greek letters

α	Significance level
ρ	Electrical resistivity (ohm-m)
κ	Thermal conductivity (W/m-K)
η	Thermal efficiency
γ	Leg aspect ratio (ratio of area to length, A/L) (mm)

Abbreviations

ANOVA	Analysis of variance
ANN	Artificial neural networks
CCD	Central composite design
DOE	Design of experiments
FEA	Finite element method
IC	Interconnect
MAE	Mean absolute error
RSM	Response surface method
TE	Thermoelectric
TEG	Thermoelectric generator
UX	Displacement in X direction

Electronic supplementary material The online version of this article (https://doi.org/10.1007/s42452-019-1120-1) contains supplementary material, which is available to authorized users.

✉ Naveen K. Karri, naveen.karri@pnnl.gov | [1]Pacific Northwest National Laboratory, 902 Battelle Blvd, Richland, WA 99354, USA. [2]Washington State University Tri-Cities, 2710 Crimson Way, Richland, WA 99354, USA.

SN Applied Sciences (2019) 1:1097 | https://doi.org/10.1007/s42452-019-1120-1

Received: 25 June 2019 / Accepted: 17 August 2019 / Published online: 26 August 2019

Subscripts

avg	Average
c	Cold side
h	Hot side
n	n-type material
p	p-type material

1 Introduction

Thermoelectric (TE) generation served as the most reliable source of electrical power and has been a preferred choice for powering space applications [1] where the reliability outweighs other performance criteria. Despite its success in the space applications and other niche applications for energy harvesting, the TE technology has not seen success in the terrestrial applications for large scale heat recovery and automobile applications. While power sources relying on TEG such as the radioisotope thermoelectric generators (RTG) employed in space applications [2, 3] operate under static conditions, the terrestrial applications typically need operation under dynamic conditions that subject the device to thermomechanical fatigue and subsequent failure [4]. Two major challenges in developing the new TE materials for most applications is the undesirably long time associated with the material development to commercialization stage [5] and device reliability [4, 6]. Currently the time it takes for a new TE material from the development phase to a successful application demonstration phase is about a decade which is typically followed by a few additional years for commercialization for device adoption. While the development of new TE materials with high figure of merit (ZT) is essential to the promotion of this technology, linking the material properties to device level performance is a key to the successful commercialization and widespread adoption of this technology [7, 8]. One of the most challenging issues often encountered during demonstrations of TEG devices developed from new materials is the device failure. The thermomechanical stresses that arise due to thermal expansion mismatch between various materials of a TEG typically lead to failure in devices designed for peak performance. The success of a new TE material is materialized only when structurally reliable devices can be made with that material and thus the development of successful TE devices needs geometry optimization from the performance and reliability perspectives. The necessity for an integrated structural and performance optimization in achieving truly optimal design is also emphasized in recent literature [9, 10]. There are several parameters that influence the performance and structural reliability of a TEG device. The geometry requirements for performance often contradict the requirements for reliability which complicates the design optimization of TEG. In one of our previous studies [11] we demonstrated these opposing geometrical requirements for the performance and reliability. The optimized TEG configurations must have a low internal resistance for better performance and reduced thermomechanical stresses for enhanced reliability.

Several studies in literature were focused on optimizing the performance of a TEG for terrestrial applications such as automotive heat recovery using analytical modeling. Hendricks et al. [12] demonstrated the complex interaction between thermal system performance and thermoelectric device optimization and focused on optimizing the system level performance of the TEG integrated with heat exchanger for vehicle energy recovery. Crane et al. [13] studies optimized the system level performance integrated with heat exchanger and focused on designs to maximize performance of a TEG with a dynamic thermal power source such as automobile exhaust. Kumar et al. [14] work focused on optimizing a TEG for automobile waste heat recovery considering the temperature dependent material properties and concluded that careful selection of leg height and area ratio (An/Ap) are important for optimal power and material requirements. Montecucco et al. [15] characterized the performance of TEGs with constant thermal power in a waste heat application where the maximum available heat is limited at any time.

Apart from performance some literature studies focused on investigating the operational stresses in TEGs by numerical simulations. Li et al. [16] studied the thermal stresses in a segmented thermoelectric uni-couple subjected to thermal cyclic loading by finite element method (FEM) and concluded that a functionally graded interface layer could improve reliability. Clin et al. [17] evaluated the effect of leg length, boundary conditions, and soldering alloys on a bismuth telluride module and concluded that the boundary conditions on the ceramic substrate and mechanical strength of the soldering alloys significantly affect stresses in the TEG components. Turenne et al. [18] simulated the steady state operational behavior of TE modules using FEA and concluded that thin modules typically produce very high stress levels at leg corners and the end constraints that subject the module to compressive stress could reduce failure. Studies also showed that the leg geometry influences stresses and performance of a TEG. Al-Merbati et al. [19] examined the influence of pin geometry on the stress levels in a TEG device subject to thermal cyclic loading and concluded that geometric configuration has significant influence on the stress levels and configurations with parallel pins could result in lowest von Mises stresses.

Recently, some studies also focused on evaluating the effects of geometry on both performance and stresses in a TEG. Erturun et al. [20] investigated the effect of various leg

geometries on thermo-mechanical and power generation performance of thermoelectric devices, and concluded that cylindrical legs could reduce the peak equivalent stresses and varying thermoelectric leg geometry can be considered as a factor for reducing overall stresses in a TEG module. Bakhtiaryfard et al. [21] considered design modification to elements to reduce thermal stresses in the modules. Fan et al. [22, 23] studied the influence of geometric dimensions, number of couples on the performance and mechanical reliability of annular TEGs. Their study concluded that the number of couples has little influence on the stresses whereas the leg length and angle ratio has significant influence on the performance and stresses of annular TEG.

While much of the cited literature focused on optimizing the performance or reducing the thermomechanical stresses in a TEG the studies focused on integrated structural reliability and performance optimization of a TEG are scarce. Some studies considered this aspect but they did not define reliability pertinent to TEGs. They focused on reducing the equivalent or von Mises stresses which usually do not correlate to the failure of brittle TE materials. For instance, Jia et al. [24] used 3D finite element models to simulate the TE and mechanical behaviors of segmented thermoelectric devices and determined optimal operating conditions for balanced TE and mechanical performances. Erturun et al. [25] studied the variation of performance and stresses with leg spacing and dimensions using design of experiments approach and demonstrated parameter selection for a target performance. Their study did not optimize the stresses or relate stresses to reliability which is necessary to estimate the tradeoff in performance while arriving at truly optimal and reliable TEG configurations. In our previous study [26] we addressed the challenge of linking the TEG leg stresses to reliability using statistical brittle material failure theory and demonstrated that the failure probability of TEG approaches zero at a certain length or aspect ratio (the ratio of length to area L/A of *p*- and *n*-type legs). Any improvement beyond that limit will only diminish the performance, especially the power output, and it is necessary to have insights on such aspect ratios to limit the tradeoff in the performance of an optimized TEG configuration. In that study we also investigated the influence of geometry, metallization and operating conditions on the reliability of a TEG and identified the parameters that significantly influence the reliability of a TEG. In the present study we focused on the simultaneous optimization of the parameters critical to the performance and reliability of a TEG. The optimization of multiple responses each of which in turn depend on multiple independent parameters was carried out using design of experiments (DOE) based response surface methodology (RSM). The DOE based approach to study the influence of geometric parameters on the performance and stresses in a TEG was considered in the study by Erturn et al. [25] that used RSM and artificial neural networks (ANN) techniques. Recently, Kishore et al. [27] used Taguchi and ANOVA techniques to optimize the performance of a TEG with external load and heat exchanger parameters.

In this study we investigated the effect of leg aspect ratios and metallization thickness on the performance and reliability of a TEG. The performance and thermomechanical stresses that affect the reliability of a TEG are simulated using finite element analysis (FEA) and the reliability under simulated stresses is quantified using statistical brittle material reliability theory and procedure discussed our previous article [24]. The DOE based RSM with face-centered central composite design (CCD) was used to fit second order quadratic regression models for the power output (P), efficiency (η), the probability-of-failure (P_f) and their simultaneous optimization. The factors and ranges for the CCD were chosen based on a two-level full-factorial effects screening study as well as the insights from the one-factor-at-a-time analysis conducted in our previous study [26].

2 Single couple finite element model

Numerical simulations were carried out to simulate the performance and the thermomechanical stresses of a single couple TEG using the commercial FEA software ANSYS [28]. The probability-of-failure (Reliability, $R = 1 - P_f$) was estimated using a macro implemented within ANSYS via ANSYS Parametric Design Language (APDL) whose details are presented in our previous work [26]. The thermoelectric and subsequent thermomechanical simulations were sequentially performed in ANSYS where the thermoelectric performance is solved first using SOLID226 elements with only TEMP and VOLT degrees of freedom (DOF), and the resulting temperatures distributions are later imposed on a structural model with SOLID186 elements that have only displacement DOFs (UX, UY, UZ). Such a sequential analysis was found to be computationally efficient compared to a coupled-field analysis with SOLID226 elements with all 5 active DOF and both thermoelectric and structural boundary conditions imposed simultaneously.

The single couple FEA model is similar to the fixed case TEG couple considered in [24]. Figure 1 illustrates the details of the single couple 3-D FEA model (front view) with typical square section legs. The couple consists of *p*- and *n*-type TE elements thermally connected in parallel and electrically in series joined by copper interconnects (ICs). A constant property couple made of *p*- and *n*-type bismuth-telluride based materials with the thermoelectric properties [29] at an average temperature of

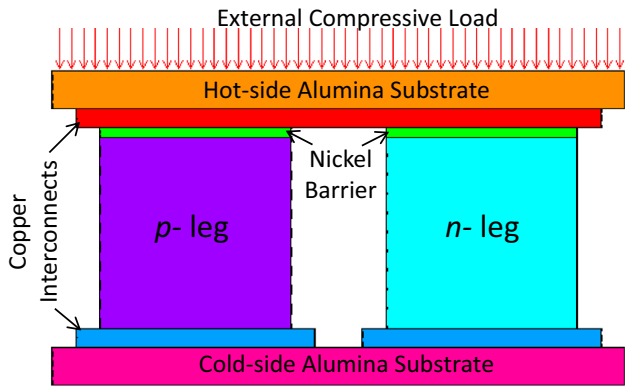

Fig. 1 FEA model configuration of a single couple TEG

~ 175 °C is considered in all the analyses. The temperature dependence of material properties is not considered in the simulation as the main intent of the study is to investigate the influence of geometrical parameters. Inclusion of temperature dependence may overshadow the minor influences from some geometrical parameters. The error in the performance parameters (power and efficiency) due to the temperature independent assumption within the temperature range 100–250 °C considered in this work was verified to be less than 10%, which is in good agreement with the literature [29]. The constant property assumption is also justified per recommendations for temperature dependent material property consideration in [30]. The error in structural performance (failure probability) shall be negligible as there is little variation in the mechanical properties of the ceramic and metallic TEG materials in the temperature range considered in this study. A diffusion barrier made of nickel (Ni) on the hot-side, typically found in medium (250 to 650 °C) to high temperature (> 650 °C) couples is include in the models. The copper ICs at the bottom and top are assumed to be bonded to ceramic substrates made of alumina. The bonding layer (solder etc.) at the interface of ICs and different TE materials are not considered and instead a thicker diffusion barrier is modeled. To investigate the potential for plastic strains in metallization, the Cu ICs and Ni barrier are modeled as elastoplastic materials with bilinear isotropic hardening behavior. The material properties and constitutive models of the single couple TEG models considered in this work are similar to those considered in [11, 26]. A load resistance between the end terminals is specified in the single couple models using a CIRCU124 element. The details of the TE materials, metallization and the substrate and the thermoelectric and mechanical properties of all the materials used in the FEA are presented in [26].

For the thermal boundary conditions, the single couple models are specified with a hot-side temperature of 250 °C and a cold-side temperature of 100 °C which results in a ΔT of 150 °C and an average temperature of 175 °C. The structural boundary conditions are specified at the bottom surface of the cold-side substrate. All the bottom surface nodes are constrained in vertical direction (UY = 0) and the minimal in-plane boundary conditions (UX = UZ = 0 at back left corner node and UZ = 0 for back right corner node) are specified at the bottom surface of the cold-side substrate to avoid rigid body rotation in the simulations. A reference temperature (TREF in ANSYS) that is the average of TEG hot and cold-side temperatures is specified in the models. Once the thermomechanical stresses are simulated, the reliability of the brittle TE materials are estimated using the Weibull statistical parameters listed in Table 1. The derivation and source data for these parameters are presented in [11].

3 Design of experiments (DOE) approach

DOE is a systematic procedure that relies on mathematical and statistical methods to analyze and/or optimize the output (referred as responses) of processes that depend on one or more independent input variables (referred to as factors). DOE has significant advantage over traditional one-factor-at-a-time analysis as carefully designed experiments could provide invaluable insights on the effects of varying inputs on the output parameters with limited number of experiments thereby saving substantial amount of time and resources during a new product or process development. The DOE implementations typically require personnel with expertise in the concerned product or process development in order to yield effective results. Optimization using DOE approach is usually a three-step process;

Table 1 Weibull parameters used in the component reliability estimations with FEA

Material	Weibull characteristic strength, σ_θ (MPa)	Weibull modulus, m (Unitless)	Weibull material scale parameter, σ_0 [Pa $(m^3)^{1/m}$]
p-type bismuth telluride	80	10	9,389,156
n-type bismuth telluride	80	10	9,389,156

- First is to identify the input parameters (factors) which significantly influence the desired output (response). This step is called effects screening.
- The second step involves fitting empirical models for studying the ranges (levels) for the critical factors to arrive at the combination of factor levels that optimize the desired responses.
- The third step typically involves confirmatory experiments.

The first step in the DOE is usually accomplished by two-level fractional factorial, full-factorial or Plackett–Burman designs. Insights and limitations of the product or process under development will assist in selecting the level of various factors during this step. The second step is accomplished by multivariate optimization techniques such as response surface methodology (RSM) which includes central composite and Box–Behnken designs, robust parameter designs such as Taguchi Arrays, mixture designs and also higher level (> 2) full-factorial designs. This step relies on fitting empirical relations that satisfactory describe the process in a limited design space (in the vicinity of optimum conditions) arrived using step one. In this work we estimated the significance of inputs using two level full factorial designs and subsequently used RSM for simultaneous optimization of multiple responses with contradicting input requirements (factor levels).

3.1 Factorial design for effects screening

Compared to the traditional one-factor-at-a-time approach, the factorial designs provide valuable information on the significance of various input parameters with a limited number of experiments or simulations. In addition to the main effects typically obtained from the one-variable-at-a-time approach (where all other variables are kept constant), the factorial designs provide interaction effects as an added advantage [31]. In our previous article we considered the effect of various input parameters on the reliability of a TEG using one-factor-at-a-time approach that necessitated hundreds of simulations. Despite knowing the influence of a specific parameter, optimization of a design with such approach is cumbersome as the relative influence of each parameter on the desired response is not quantified. In this work we studied the effect of similar parameters for their significance as well as quantified their influence using two-level full factorial designs. A full-factorial design with 'n' factors at two levels requires 2^n simulations. For screening the effect of 6 variables in the current study we conducted a total of $2^6 = 64$ simulations. The full-factorial designs were run to obtain the main, two-way, and higher order interaction effects when necessary. Sometimes, fractional factorial simulations are sufficient to provide most of the main and two way interaction effects [31]. The parameters (factors) studied for screening are the leg height, the p-leg area, the n-leg area, leg spacing (d), diffusion barrier thickness, and copper interconnect thickness. Tables 2 and 3 present the factors and their levels used in the screening effects study. Two sets are analyzed during the screening process to obtain a better understanding on the contribution of factors and their interactions, especially the leg lengths and metallization thicknesses, as discussed in the results section.

Table 2 Factors and levels considered in the 2-level full-factorial screening analysis set #1

Factor	(–) Low level (mm)	(+) High level (mm)
Leg length (L)	2.5	7.5
p-leg width (Wp)	5	6.2
n-leg width (Wn)	4	5
Leg spacing (D)	1	4
Cu interconnect thickness (tIC)	0.2	1
Diffusion barrier thickness (tBar)	0.1	1

Table 3 Factors and levels considered in the 2-level full-factorial screening analysis set #2

Factor	(–) Low level (mm)	(+) High level (mm)
Leg Length (L)	5	10
p-leg width (Wp)	5	6.2
n-leg width (Wn)	4	5
Leg spacing (D)	1	4
Cu interconnect thickness (tIC)	0.2	1
Diffusion Barrier thickness (tBar)	0.05	1

The factor levels for the effects screening simulations are generally chosen based on the prior knowledge of the system or process to avoid the real-time limitations of design and fabrication. Such a selection provides better insights on the contribution of the factor on a desired response compared to randomly varying levels in a wide range. For instance the factor levels for the widths of p- and n-legs are chosen such that the cross section area of p-leg is always greater than or equal to the n-leg area. This is based on the knowledge that for a TEG designed for optimal efficiency or power density the ratio An/Ap should be 0.81 and 0.88 according to the Eqs. (1) and (2), respectively. Also, in order to avoid significant deviation from the square cross section, the widths are not significantly varied from the depths (5 mm for both legs).

Area ratio for optimal efficiency of a TEG, $$\frac{\gamma_n}{\gamma_p} = \left(\frac{\rho_n \kappa_p}{\rho_p \kappa_n}\right)^{1/2} \quad (1)$$

Area ratio for optimal power density (per total area), $$\frac{\gamma_n}{\gamma_p} = \left(\frac{\rho_n}{\rho_p}\right)^{1/2} \quad (2)$$

The processing conditions (reference state) and the external compressive load that were found to influence the structural reliability in our previous study were not studied and are kept constant in the simulations. Inclusion of those two additional variables would have required 256 runs in a full-factorial design simulation. With the insights from our previous study, the stress frees state (TREF in ANSYS) is considered as the average operating temperature and a constant compressive load of 3 MPa was applied on the top substrate.

3.2 Response surface methodology

Response surface methodology (RSM) is a collection of mathematical and statistical techniques employed for modeling and analysis of problems in which the desired response(s) are influenced by several variables and the objective is to optimize those responses [31]. RSM typically involves fitting empirical models using regression models. To start with RSM, a first order model as described by Eq. (3) is usually fit in some region of independent variables which provides a sense of direction towards the optimum conditions. Then, using the method of steepest ascent (procedure to move in the direction of maximum increase in response) or method of steepest descent if minimization is desired), the vicinity of optimum condition/s could be determined.

$$y = \beta_0 + \beta_1 x_1 + \beta_2 x_2 + \cdots + \beta_k x_k + \varepsilon \quad (3)$$

where y is the desired response, β_i are the regression coefficients, x_i are the independent variables and ε is a random error.

Once the vicinity of optimum conditions is found, the optimum conditions are usually determined by fitting more precise higher order models such as the second order response surface model described by Eq. (4). For most cases such a second order response is adequate to satisfactorily capture any curvature in the responses and in some limited cases a third order model involving cubit terms may be needed to describe the nonlinearity associated with the response [32].

$$y = \beta_0 + \sum_{i=1}^{k} \beta_i x_i + \sum_{i=1}^{k} \beta_i x_i^2 + \sum \sum_{i<j=2}^{k} \beta_{ij} x_i x_j + \varepsilon \quad (4)$$

While a response surface models could be fit to several DOE designs including the factorial designs, there are specific designs called response surface designs (RSD) for fitting the response surface that are far more superior than fitting surfaces to factorial designs. The most widely used RSDs are the Box–Behnken Design and the Central Composite Design (CCD). In this work we employed CCD with face-centered axial (star) points to fit the surfaces for three desired responses.

4 Results and discussion

4.1 Effects screening with 2^k full-factorial runs

As discussed in the "Factorial Design" section, full factorial designs with six factors at two levels listed in Table 1 are initially simulated to understand the effect of those factors on each of the three desired responses for a TEG i.e., the power output, thermal efficiency, and the probability-of-failure (P_f).

One of the significant findings from our previous one-factor-at-a time studies [26] was the difference in performance, stress distributions, and peak stresses in the metallization and TE legs at different leg lengths. Short lengths are preferred for high power and longer legs are preferred for efficiency and reliability for typical applications where external load resistance is usually higher than the internal resistance of TEG system. Once the designs deviate from optimum performance aspect ratios (L/A) due to variation in length, the relative drop in power is significantly higher compared to efficiency initially [11]. Hence the contribution of leg length to performance parameters power and efficiency could differ at shorter length ranges (2–5 mm) compared to longer ranges (5–10 mm). Also, at relatively short lengths (~ 2.5 mm) compared to metallization thickness (0.25–1 mm), significant high stresses were observed in the metallization that ultimately resulted in plastic strains especially in the diffusion barrier material. Despite low strains (≪ 1%) such designs could lead to metallization failure under thermal cycling (fatigue) in application such as energy recovery from automobile exhaust. At relatively longer leg lengths, the metallization were free of plastic strains and the effect of their thickness was pronounced. To analyze the aforementioned differences in influences at different length ranges, an additional screening set of simulations with factors and levels listed in Table 2 were

Table 4 Set #1 results least square fit summary table

Source	LogWorth	PValue	
L(2.5,7.5)	107.252	0.00000	
Wp(5,6.2)	64.326	0.00000	
Wn(4,5)	64.326	0.00000	
Wp*Wn	17.870	0.00000	
tIC*tBar	11.304	0.00000	
tIC(0.2,1)	8.698	0.00000	^
tBar(0.1,1)	8.616	0.00000	^
L*Wp	7.093	0.00000	
L*Wn	7.093	0.00000	
L*tIC	2.247	0.00566	
L*tBar	1.815	0.01532	
D*tBar	1.665	0.02162	
D*tIC	1.440	0.03631	
Wp*tIC	0.927	0.11817	
Wp*D	0.441	0.36221	
Wn*tBar	0.311	0.48876	
Wp*tBar	0.254	0.55752	
Wn*D	0.194	0.63957	
D(1,4)	0.151	0.70702	^
Wn*tIC	0.112	0.77221	
L*D	0.000	0.99990	

^Beside "P value" column values denote effects with containing effects above them

Table 5 Set #2 results least square fit summary table

Source	LogWorth	PValue	
L(5,10)	134.076	0.00000	
Wp(5,6.2)	100.026	0.00000	
Wn(4,5)	100.026	0.00000	
L*Wn	66.783	0.00000	
L*Wp	66.783	0.00000	
Wp*Wn	54.645	0.00000	
tBar(0.05,1)	11.516	0.00000	
tIC*tBar	11.180	0.00000	
tIC(0.2,1)	10.898	0.00000	^
L*tBar	7.351	0.00000	
L*tIC	6.986	0.00000	
d*tIC	0.186	0.65122	
Wn*tIC	0.075	0.84152	
L*d	0.067	0.85801	
Wp*tBar	0.042	0.90783	
d(1,4)	0.042	0.90783	^
Wn*tBar	0.042	0.90783	
Wn*d	0.026	0.94126	
Wp*tIC	0.019	0.95803	
d*tBar	0.011	0.97481	
Wp*d	0.011	0.97481	

^Beside "P value" column values denote effects with containing effects above them

also conducted. Alternatively, one could consider a 3-level full or fractional factorial designs or a combined (some factors at 2-level and other at higher levels) which could necessitate a higher number of simulations. The results data (P, η, and P_f) from both the effect screening simulation sets are presented in Tables 14 and 15 included in the supplemental material.

To estimate the significance of factors and their interactions on the desired responses, the results from the DOE full-factorial screening data sets were analyzed with commercial statistical modeling and analysis software JMP [33]. The least squares fit overall effect summary which lists the minimum *p* value among the *p* values for any effect (from multiple responses) based on the results from Set #1 and Set #2 factorial runs are summarized in Tables 4 and 5 respectively. In these tables the Source term indicates the main or interaction effect and the Log Worth statistic (defined as −log(*p* value)) represents the significance of a main or interactions effect. A LogWorth greater than 2 (indicated by the blue dashed line) is considered statistically significant for inclusion of a factor at 1% significance level. The probability (*p* value) listed in the tables is the minimum for that source term from the three responses studied. The effect summary from both the Tables 4 and 5 indicate that ten of the of the regression model terms from Set #1 and 11 terms from Set #2 are significant at α = 0.01 level (LogWorth > 2). These terms are primarily the main and interaction effects of the factors; L, Wp, Wn, tIC, tBar.

The summary of fit, analysis of variance (ANOVA) and parameter estimates for all the three individual responses; power, efficiency and probability-of-failure, are included in the supplemental material (Tables 16 through 21). In these tables the terms R^2 represents the adequacy of fitted models and a value close to 1.0 indicates that the models fit the data well. The adjusted R^2 represents the impact of changing the number of model terms. The parameter estimates represent the coefficients of the regression fits to the data. These parameter estimates are shown in coded terms (low level − 1 and high level + 1) to provide insights on the magnitude of effect for the main and interaction terms. The F-Ratio is the test statistic used to determine whether any term in the model influences the response. A large F-Ratio indicates statistical significance. The probability (Prob > F) in the ANOVA tables (sometimes referred as the *p* value) less than or equal to the significance level (α = 0.05) indicates the fitted model appropriately describes the variation in response. Similarly, the probability (Prob > |t|) in the parameter estimates tables indicates that the model term significantly contributes to the response (when highlighted).

From the overall summary in Tables 4, 5 and the individual response summary Tables 16 through 21 included in the supplementary material, it is evident that the p and n-leg lengths, areas (i.e., widths Wp and Wn with the same depth), and the metallization thicknesses (tIC and tBar) are the influential factors for performance and reliability. It is important to note that apart from the main effects, the interactions are also found to be significant. While the interaction between the metallization thicknesses i.e., the interconnect and diffusion barrier thickness combination is significant for reliability (tIC * tBar in Tables 20, 21 in the supplemental material), the interaction between length and width (or area) turned out to be significant for power and efficiency as one would expect. The relative contribution of each of the main and interaction effects are summarized in Table 6. These percentage contributions are the

Table 6 Percentage contribution of terms based on the results from Set #1 and Set #2

Source	From set #1 results data			From set #2 results data		
	Power [W] (%)	Efficiency (%)	P_f (%)	Power [W] (%)	Efficiency (%)	P_f (%)
L	98	91	61.2	95	86	13.2
Wp	1	1	1.6	2	2	0.0
Wn	1	1	0.0	2	2	0.0
d	0	0	0.0	0	0	0.0
tIC	0	0	8.8	0	0	20.8
tBar	0	0	8.7	0	0	23.0
L*Wp	0	4	1.3	0	5	0.0
L*Wn	0	3	0.0	0	5	0.0
L*d	0	0	0.0	0	0	0.0
L*tIC	0	0	1.3	0	0	10.1
L*tBar	0	0	1.0	0	0	10.9
Wp*Wn	0	0	0.0	0	1	0.0
Wp*d	0	0	0.1	0	0	0.0
Wp*tIC	0	0	0.4	0	0	0.0
Wp*tBar	0	0	0.1	0	0	0.0
Wn*d	0	0	0.0	0	0	0.0
Wn*tIC	0	0	0.0	0	0	0.0
Wn*tBar	0	0	0.1	0	0	0.0
d*tIC	0	0	0.7	0	0	0.1
d*tBar	0	0	0.9	0	0	0.0
tIC*tBar	0	0	13.8	0	0	21.8

rough estimates obtained from the relative magnitudes of sum of the squares of each factor or interaction. The summary Tables 4 and 5 in conjunction with the Parameter Estimates Tables 16 through 21 provided in the supplemental material could be used to confirm the magnitude of these effects. The difference in percentage contributions estimated from the data sets #1 and #2 (from Tables 4, 5 respectively) demonstrate the importance of choosing appropriate levels even during screening. Random selection could lead to incorrect conclusions on the choice of factors and levels required for subsequent optimization design space.

An interesting observation is that despite differences in the percentage contributions from the datasets, the influence trends of main and interaction effects turned out to be the same for all the responses except for the effect of length on efficiency. The parameter estimate tables presented in supplemental material (Tables 16 through 21) lists the regression coefficients which provide insights on the trends related to each factor. A positive estimate indicates that the desired response increases with the factor and vice versa. If we consider leg length (L), the estimate for power and probability of failure (P_f) are –ve from both sets indicating the output power and probability of failure decreases with leg length. On the other hand, the L estimate for efficiency is +ve from set #1 (which includes short length) indicating efficiency increases with length and turned out to be –ve from set #2 contradicting the observation from set#1. Such results typically indicate curvatures in response which cannot be captured by a 2-level factorial design. It is important to include the levels of factors that produce such peaks to optimize responses in subsequent higher order analysis. The existence of curvature in efficiency response could be attributed to the ratio of internal to external load resistance (R/R_0) which varies with leg length. From the established theory for performance optimization we know that a peak power is obtained at matching load resistance $R/R_0 = 1.0$, whereas the peak efficiency is attained at $R/R_0 = \sqrt{(1 + ZT)}$ where ZT is the couple figure-of-merit.

4.2 Response surface analysis

The effect screening analyses presented in the previous section indicated that except for the leg distance, the other 5 out the 6 factors considered are significant for either performance or reliability. However, a careful analysis of the parameter estimates concludes those five factors could be reduced to three by utilizing the interaction effect between the factors. For instance instead of varying Wp and Wn separately, the ratio Wn/Wp could be varied based on the requirements for optimal power and efficiency described by Eqs. (1) and (2). Similarly the net effect of diffusion barrier and interconnect thickness could be captured by varying the ratio tBar/tIC below and above

1.0. Such a variation implicitly captures the effect of both parameters and simplifies the optimization process. In this work we achieved the variability of Wp/Wn and tBar/tIC by keeping the Wn and tIC constant and then varying only Wp and tBar respectively.

A face-centered central composite design with eight cube points, one center point, six axial points with no replicates requiring 15 total runs was used to obtain the empirical relations that describe the desired responses accurately in the domain of interest for optimal factors. Table 7 presents the factors and levels considered for response surface analysis. Because of the face-centered cube design where the axial or star point lie at the center of the cube faces, each factor was evaluated at three levels as presented in Table 8.

The fitted surfaces for the response power, efficiency and probability of failure in terms of uncoded factors are described by Eqs. (5) (6) and (7) respectively. The creation of quadratic response surface regression models with least-square fitting method and the analyses of the fitted response surfaces were carried out using the statistical analysis software JMP. The surface plots of predicted responses by the RSM models are presented in Fig. 2. It is evident from these response contours that the power and efficiency vary with leg length and width, with length having significant influence. On the other hand, all the three factors (leg length, width and barrier thickness) have significant effect on the probability of failure.

$$P = 0.27164 - 0.064242L + 0.02696W_p - 0.00012tBar + 0.003955L^2 - 0.001531W_p^2 0.00023tBar^2 + 0.000358L \times W_p + 0.000000L \times tBar + 0.000000W_p \times tBar \quad (5)$$

$$\eta = 0.02954 + 0.009667L + 0.000477W_p - 0.000046tBar - 0.001231L^2 - 0.000291W_p^2 + 0.000091tBar^2 + 0.000536L \times W_p + 0.000000L \times tBar - 0.000000W_p \times tBar \quad (6)$$

$$P_f = 0.980 - 0.3783L - 0.054W_p + 0.342tBar + 0.06841L^2 + 0.0255W_p^2 - 0.012tBar^2 - 0.04522L \times W_p - 0.0987L \times tBar + 0.0256W_p \times tBar \quad (7)$$

The overall effects summary which lists the minimum p value among the p values for any effect (from multiple responses) is presented in Table 9. The least-square

Table 7 Factors and levels for the central composite design (CCD)

Factor	(–) Low level (mm)	(+) High level (mm)
Leg length (L)	2.5	5
p-leg width (Wp)[a]	5	6.2
Diffusion barrier thickness (tBar)[b]	0.05	0.45

[a]Varied with Wn kept constant at 5 mm such that Wn/Wp varies from 0.81 to 1

[b]Varied with tIC kept constant at 0.25 mm such that tBar/tIC varies from 0.2 to 1.8

Table 8 Required combinations of factors and levels for face-centered CCD

Run #	Pattern	L (mm)	Wp (mm)	tBar (mm)	Power (W)	Efficiency (%)	P_f (%)
1	−−−	2.5	5	0.05	0.237	4.78	27
2	−−+	2.5	5	0.45	0.237	4.78	36
3	−+−	2.5	6.2	0.05	0.250	4.61	42
4	−++	2.5	6.2	0.45	0.250	4.61	53
5	+−−	5	5	0.05	0.155	5.56	2
6	+−+	5	5	0.45	0.155	5.56	2
7	++−	5	6.2	0.05	0.169	5.55	4
8	+++	5	6.2	0.45	0.169	5.55	4
9	a00	2.5	5.6	0.25	0.244	4.70	38
10	A00	5	5.6	0.25	0.162	5.57	3
11	0a0	3.75	5	0.25	0.189	5.36	8
12	0A0	3.75	6.2	0.25	0.203	5.27	14
13	00a	3.75	5.6	0.05	0.197	5.33	9
14	00A	3.75	5.6	0.45	0.197	5.33	11
15	000	3.75	5.6	0.25	0.197	5.33	10
Min					0.155	4.61	2
Max					0.250	5.57	53

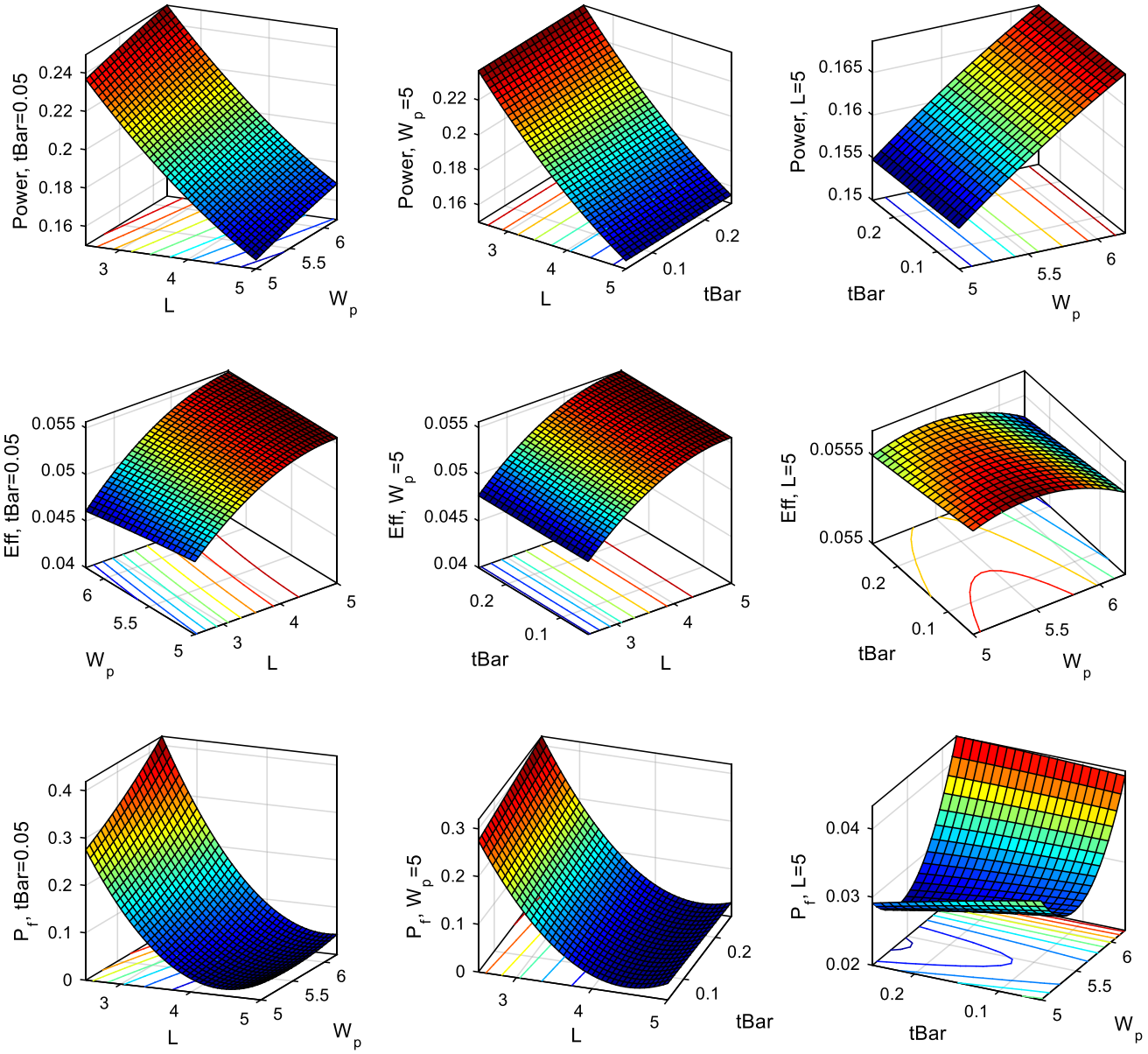

Fig. 2 Response surface plots for Power (top row), Efficiency (middle row) and Probability of Failure (bottom row) with one of the factors kept constant at a level

Table 9 RSM effects summary

Source	LogWorth	PValue
L	13.207	0.00000
Wp	9.287	0.00000
L*L	9.142	0.00000
L*Wp	6.975	0.00000
Wp*Wp	2.923	0.00119
L*tBar	2.407	0.00392
tBar	2.387	0.00410 ^
Wp*tBar	0.255	0.55634
tBar*tBar	0.086	0.82106

^Beside "P value" column values denote effects with containing effects above them

fits, ANOVA, and parameter estimates of the three fitted responses power, efficiency and probability of failure are presented in Tables 10, 11 and 12 respectively. The effect summary presented in Table 9 shows that seven of the quadratic model terms are significant at $\alpha = 0.01$ level (LogWorth > 2). The fit summary presented in Tables 11, 12 and 13 show that the R^2 and adjusted R^2 (represents the impact of changing the number of model terms) for all the responses are greater than 0.99. R^2 represents the adequacy of fitted models and a value close to 1.0 indicates that the models fit the data well. The parameter estimates that represent the coefficients of the quadratic regression equations are also presented in the Tables 10, 11 and 12. These parameter estimates are shown in coded terms (low level -1 and high level +1) to provide insights on the

Table 10 Summary of fit, ANOVA and parameter estimates for power

Summary of fit—power				
RSquare				0.999992
RSquare Adj				0.999978
Root mean square error				0.000163
Mean of response				0.200596
Observations (or sum wgts)				15
Anova				
Source	DF	Sum of squares	Mean square	F ratio
Model	9	0.01714691	0.001905	71560.41
Error	5	0.00000013	2.662e−8	**Prob > F**
C. Total	14	0.01714704		< .0001*
Parameter estimates				
Term	Estimate	SE	t Ratio	Prob > |t|
Intercept	0.1968366	8.77e−5	2244.4	< .0001*
L	− 0.040717	5.16e−5	− 789.1	< .0001*
Wp	0.0066948	5.16e−5	129.75	< .0001*
tBar	0	5.16e−5	0.00	1.0000
L * Wp	0.0002683	5.769e−5	4.65	0.0056*
L * tBar	0	5.769e−5	0.00	1.0000
Wp * tBar	0	5.769e−5	0.00	1.0000
L * L	0.0061802	0.000102	60.74	< .0001*
Wp * Wp	− 0.000551	0.000102	−5.41	0.0029*
tBar * tBar	9.2222e−6	0.000102	0.09	0.9313

*Beside "Prob>|t|" column values (whenever less than the chosen significance level α = 0.05) indicates that model term is significant. Probabilities less than 0.01% are defaulted to 0.01%

magnitude of effect for the main and interaction terms. The coefficients in uncoded terms as shown in Eqs. (5)–(7) thus differ from those presented in the tables. The F-Ratio is the test statistic used to determine whether any term in the model influence the response. A large F-Ratio indicates statistical significance. The probability (Prob > F) in the ANOVA tables (sometimes referred as the *p* value) less than or equal to the significance level (α = 0.05) indicates the fitted model appropriately describes the variation in response. Similarly, the probability (Prob > |t|) in the parameter estimates tables indicates that the model term significantly contributes to the response.

4.3 Simultaneous optimization of multiple responses

The results from the screening studies showed that several factors influence the desired responses; hence, it is necessary to simultaneously optimize all the desired responses for the choice of factors. Simultaneous optimization of multiple responses that depend on multiple factors is not an easy procedure. Various options are available for simultaneous optimization of multiple responses depending on the number of factors and responses. When there are few factor and responses, straightforward techniques such as contour plot overly could be used where one could arrive at optimal conditions by visually examining the responses under variation of one or two factors with others kept at constant levels. This method suffers from tediousness when there are more factors and responses as it requires trial and error approach to determine which factors to hold constant and at what levels for the best view of a response surface.

Another technique is to formulate the problem as a constrained optimization problem and solve those using nonlinear programming methods and numerical optimization algorithms. A popular approach to optimization of multiple responses is to use simultaneous optimization technique that makes use of desirability functions. This technique was popularized by Derringer and Suich [34]. Here the approach is to convert each response y_i into an individual desirability function d_i that varies from 0 to 1 and then arrive at factors that maximize the overall desirability (D) that is defined as the geometric mean of

Table 11 Summary of fit, ANOVA and parameter estimates for efficiency

Summary of fit—efficiency				
RSquare				0.999984
RSquare Adj				0.999955
Root mean square error				2.542e−5
Mean of response				0.051921
Observations (or sum wgts)				15
Anova				
Source	DF	Sum of squares	Mean square	F ratio
Model	9	0.00020066	0.000022	34516.53
Error	5	3.22964e−9	6.46e−10	**Prob > F**
C. Total	14	0.00020066		< .0001*
Parameter estimates				
Term	Estimate	SE	t Ratio	Prob > |t|
Intercept	0.05327	1.366e−5	3899.6	< .0001*
L	0.0042934	8.037e−6	534.21	< .0001*
Wp	− 0.000464	8.037e−6	− 57.72	< .0001*
tBar	0	8.037e−6	0.00	1.0000
L*Wp	0.0004015	8.986e−6	44.68	< .0001*
L*tBar	0	8.986e−6	0.00	1.0000
Wp*tBar	0	8.986e−6	0.00	1.0000
L*L	− 0.001923	1.585e−5	− 121.3	< .0001*
Wp*Wp	− 0.000105	1.585e−5	− 6.61	0.0012*
tBar*tBar	3.7778e−6	1.585e−5	0.24	0.8211

*Beside "Prob>|t|" column values (whenever less than the chosen significance level α = 0.05) indicates that model term is significant. Probabilities less than 0.01% are defaulted to 0.01%

individual desirability functions as presented by Eq. (8) for 'm' responses. If the response y_i is at its target, then $d_i = 1$ and if the response is outside an acceptable region, then $d_i = 0$. The emphasis on being close to a desired target value with desirability function could also be varied by specifying weights to the desirability functions [29–31].

$$D = (d_1 \times d_2 \times \cdots \times d_m)^{\frac{1}{m}} \tag{8}$$

We used this desirability function approach to simultaneously optimize the power, efficiency and reliability of a TEG using JMP software. Figure 3 presents a case of optimized solution (maximized power, efficiency and minimized P_f) under the constraints specified in Eq. (9). This is a case where high reliability ($P_f \leq 5\%$) is desired. The maximized overall desirability D for this case is about 0.91and the factor level settings of leg length, P-leg width and barrier layer thickness for this optimal design are 4.1 mm. 5.12 mm and 0.05 mm respectively. Several other factor combinations could also satisfy the constraints specified in Eq. (9) but the overall desirability obtained with such other combinations will be less than or equal to the maximized desirability 0.91. For instance, the unshaded white region of the overlaid contour plot presented in Fig. 4 represents the domain for such other potential solutions. The dots around the response contour lines presented in Fig. 4 provide the direction of increase for that response.

$$\textbf{Case \#1}: \quad \text{Maximize D for } P_f \leq 5\%, \quad P \geq 180\ \text{mW and } \eta \geq 5\%. \tag{9}$$

Another case of an optimal solution where slightly higher power output and efficiency are desired at the expense of a reduced reliability is presented in Fig. 5. In this case the solution is optimized for a minimum requirement of 200 mW and additional constraints specified in Eq. (10). A maximized desirability of 0.748 is achieved in this case. The limited other potential solutions (with tBar = 0.05 mm) that satisfy the requirements presented in Eq. (10) with a $D \leq 0.748$ are illustrated by the unshaded white region in Fig. 6.

$$\textbf{Case \#2}: \quad \text{Maximize D for } P_f \leq 10\%, \quad P \geq 200\ \text{mW and } \eta \geq 5.1\%. \tag{10}$$

Table 12 Summary of fit, ANOVA and parameter estimates for probability of failure (P_f)

Summary of fit—P_f				
RSquare				0.997603
RSquare Adj				0.993288
Root mean square error				0.013807
Mean of response				0.175534
Observations (or sum wgts)				15
Anova				
Source	DF	Sum of squares	Mean square	F ratio
Model	9	0.39665389	0.044073	231.1893
Error	5	0.00095317	0.000191	**Prob > F**
C. Total	14	0.39760706		< .0001*
Parameter estimates				
Term	Estimate	SE	t Ratio	Prob > |t|
Intercept	0.0984793	0.007421	13.27	< .0001*
L	− 0.178909	0.004366	− 40.98	< .0001*
Wp	0.0410131	0.004366	9.39	0.0002*
tBar	0.0218394	0.004366	5.00	0.0041*
L * Wp	− 0.033913	0.004882	− 6.95	0.0009*
L * tBar	− 0.024676	0.004882	− 5.06	0.0039*
Wp * tBar	0.0030755	0.004882	0.63	0.5563
L * L	0.1068837	0.00861	12.41	< .0001*
Wp * Wp	0.0091882	0.00861	1.07	0.3347
tBar * tBar	− 0.000489	0.00861	− 0.06	0.9569

*Beside "Prob>|t|" column values (whenever less than the chosen significance level α = 0.05) indicates that model term is significant. Probabilities less than 0.01% are defaulted to 0.01%

Table 13 Error analysis (extreme combinations)

Test factors and levels			From FEA			RSM prediction			Relative error			Abs Error
L (mm)	Wp (mm)	tBar (mm)	Power (W)	η (%)	$\%P_f$	Power (W)	η (%)	$\%P_f$	Power [W] (%)	η (%)	$\%P_f$	P_f (%)
3.125	5.3	0.15	0.21492	5.11	15.03	0.21532	5.09	17.15	0	0	14	2
3.125	5.3	0.35	0.21492	5.11	17.24	0.21532	5.09	20.42	0	0	18	3
3.125	5.9	0.15	0.22164	5.04	19.54	0.22188	5.03	22.80	0	0	17	3
3.125	5.9	0.35	0.22164	5.04	22.33	0.22188	5.03	26.37	0	0	18	4
4.375	5.3	0.15	0.17471	5.49	4.53	0.17447	5.50	2.19	0	0	52	2
4.375	5.3	0.35	0.17471	5.49	4.79	0.17447	5.50	2.99	0	0	38	2
4.375	5.9	0.15	0.18164	5.46	6.16	0.18130	5.48	4.44	0	0	28	2
4.375	5.9	0.35	0.18164	5.46	6.47	0.18130	5.48	5.55	0	0	14	1
								Max	0	0	52	4
											MAE =	2

4.4 Validation simulations

Validation case simulations and error analyses are performed to demonstrate the effectiveness of the DOE based RSM in predicting the responses apart from optimization. Table 13 presents the results from the error analysis. These validation runs considered the extreme combinations of factor levels to estimate maximum possible error in predictions. It is interesting to see that the models accurately

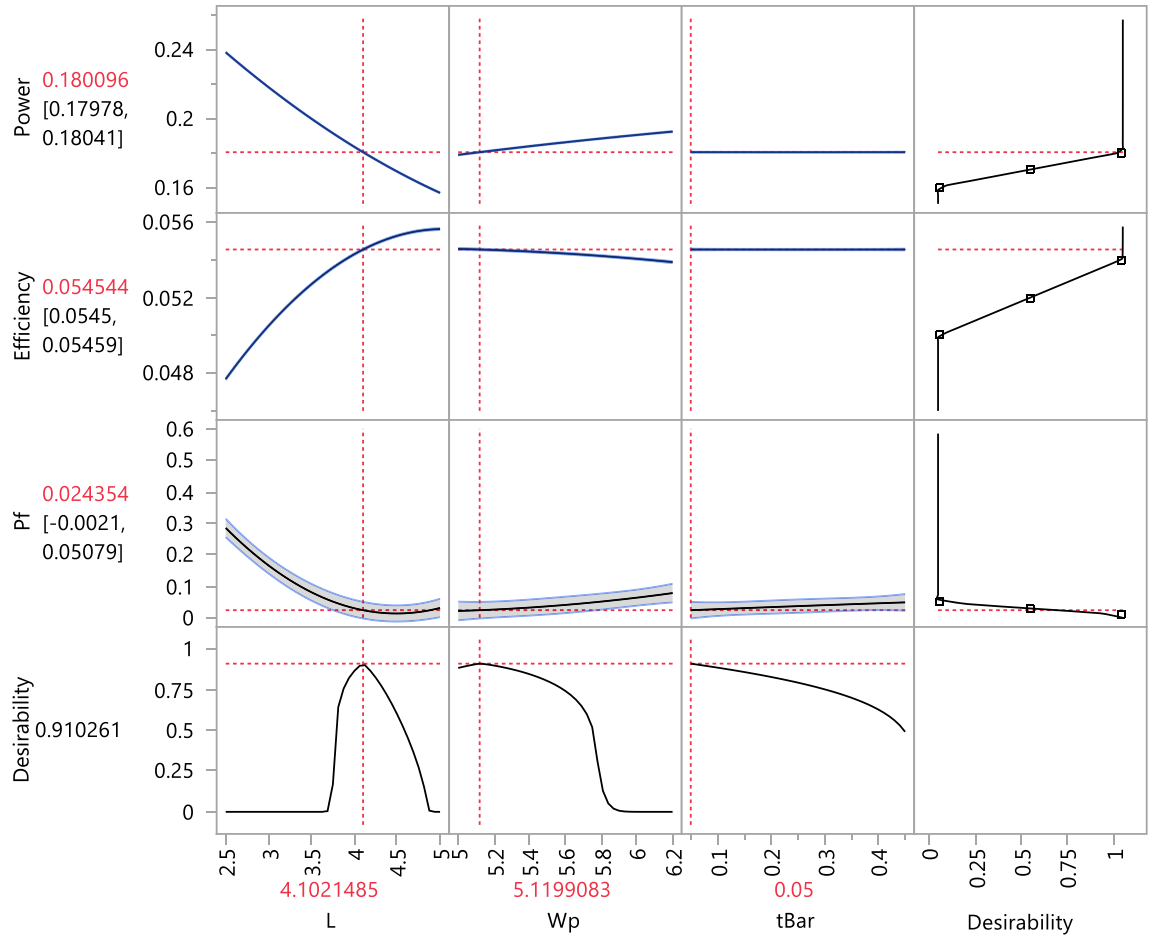

Fig. 3 Maximized desirability for Case #1 optimal solution

(< 1%) predicted the power and efficiency responses. Large relative errors are noticed in the P_f estimates < 5%, however results indicated that an absolute error and mean absolute error are more appropriate for this estimate. Such a model evaluation metric is commonly used in regression analysis [35] and RSM predictions [36] for percentage quantities. The maximum absolute error in P_f prediction is 4% and the MAE is about 2%. These results demonstrate the effectiveness of RSM approach for general predictions as well as optimization.

5 Conclusions

Integrated structural and thermoelectric design and optimization is a key to the development of structurally reliable and optimally performing TEG systems. Such an integrated approach is especially necessary to expedite the process of new TE materials development for medium to high temperature applications. The geometric parameters of a TEG affect both the performance and reliability of TEG. The geometric requirements for performance usually contradict the requirements for reliability. While relations are established to optimize the performance of a TEG based on the material thermoelectric properties, no material property based correlations exist to predict the structural integrity of a TEG which complicates the integrated design optimization process. In this work we implemented the DOE based RSM models in conjunction with FEA simulations to demonstrate an integrated optimization from reliability and performance perspectives. The parameters that significantly contribute to the performance and reliability of a TEG were initially determined using 2-level full factorial studies which also provided insights on the factor levels and domain space for subsequent optimization. The central composite design of RSM was used to fit quadratic regression models for the power output, efficiency, and the probability-of-failure of a TEG. Once the models are fit, the simultaneous multiple response optimizations were carried out using desirability functions. The following conclusion can be made from this study:

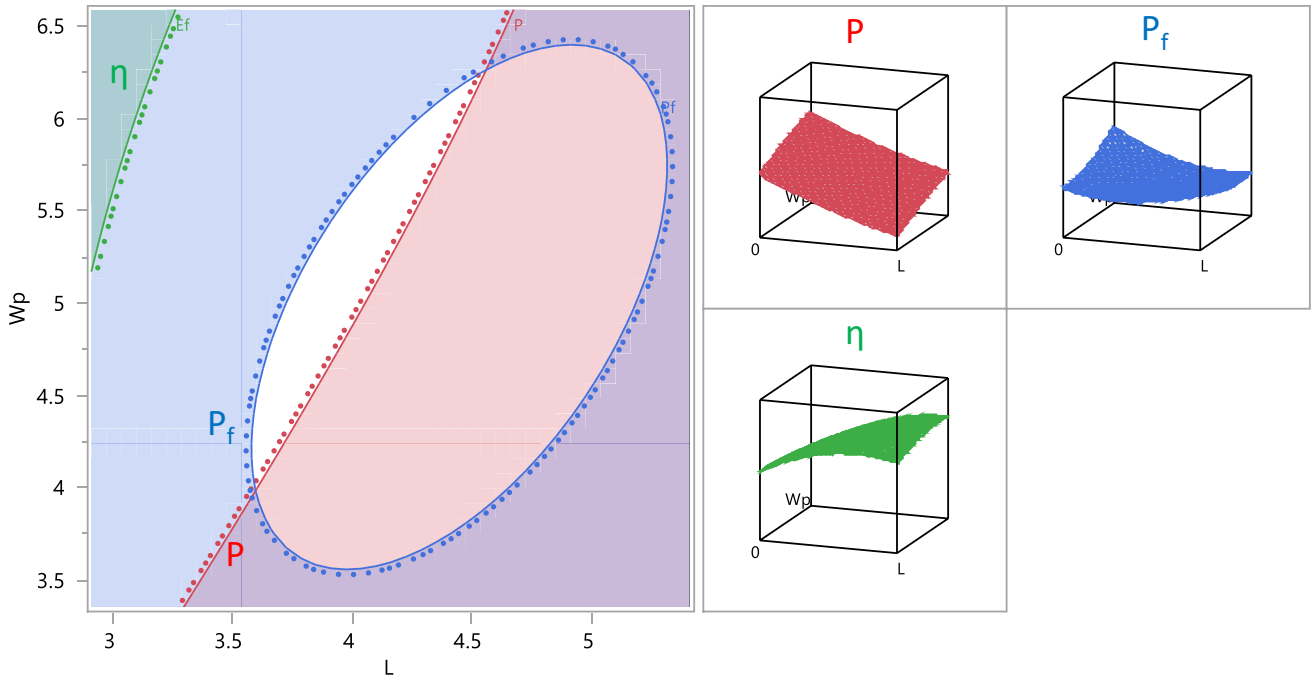

Fig. 4 Domain for Case #1 solutions (white area)

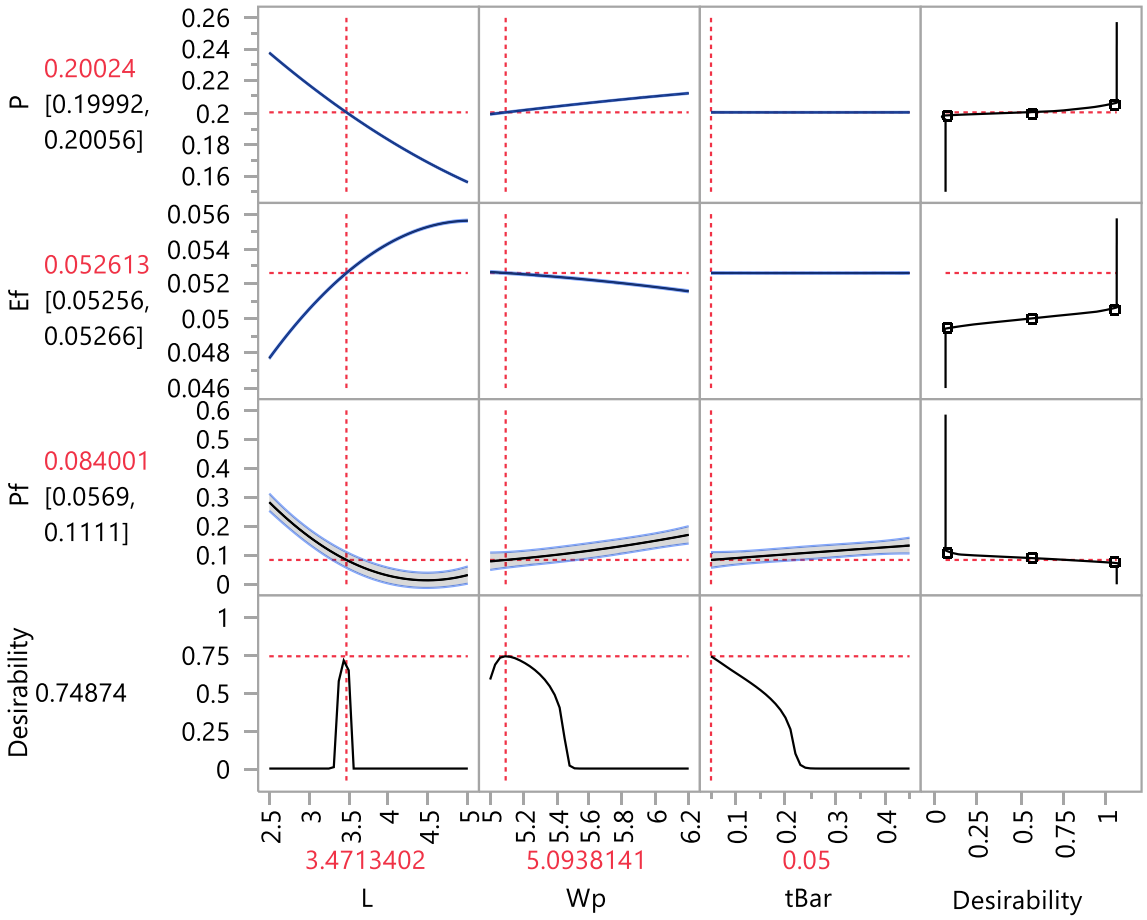

Fig. 5 Maximized desirability for Case #2 optimal solution

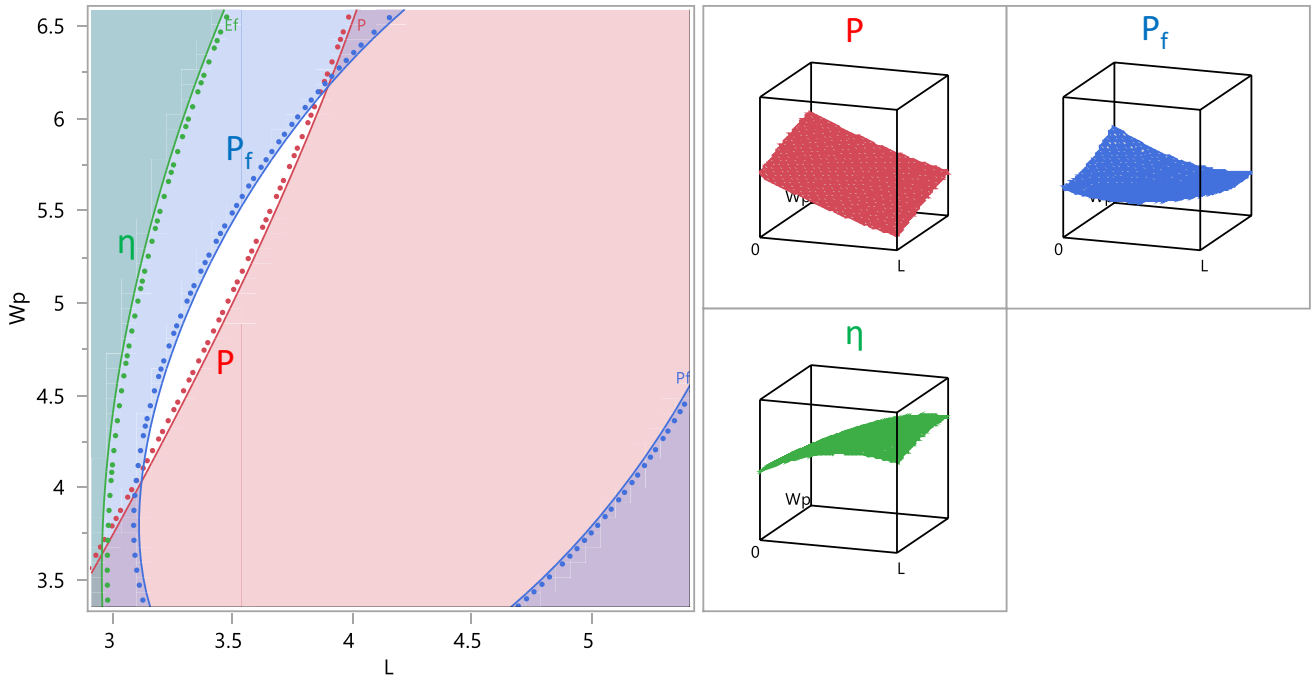

Fig. 6 Domain for Case #2 solutions (white area)

- The leg length, p- and n-type leg areas significantly influence performance whereas the leg-length, width, and metallization (interconnect and diffusion barrier layer) thicknesses impact the reliability of a TEG.
- Selection of factor levels is important to the TEG design optimization from reliability and performance aspects.
- The power of a TEG decreases with length and for typical application where the external load resistance is usually higher than the internal resistance of a TEG the efficiency increases to a point then decreases.
- The probability of failure of a leg decreases with leg length and widths under constant depths.
- A barrier layer—interconnect thickness ratio less than 1.0 is found to be preferable for interface reliability with Ni barrier and Cu interconnects.
- The influence of barrier layer and interconnect thickness on the failure probability is profound at shorter lengths ($L/W \approx 1.0$) compared to longer lengths ($L/W \approx 2.0$).
- The DOE based RSM model with desirability functions is an appropriate choice for simultaneous multiple response optimization and for estimating the trade-offs between performance and structural reliability of a TEG.
- The RSM models accurately predicted the power and efficiency responses and satisfactorily (difference < 5%) predicted the failure probabilities.
- The domain for optimal designs from the reliability and performance aspects of a TEG could be small and depends on the optimization constraints.

The DOE based approach appears to be a robust technique that could be integrated into the TE material development and device manufacturing processes to reduce the lengthy times (currently more than a decade) between the material development and device commercialization stages.

Acknowledgements The authors would like to thank the Pacific Northwest National Laboratory (PNNL) for providing the educational assistance and computational resources needed for the work performed in this study. The authors would also like to thank Dr. Brian Koeppel from PNNL for the technical review and comments on the structural analyses and DOE based methodology presented in this work.

Compliance with ethical standards

Conflict of interest The authors declare that they have no conflict of interest.

References

1. Bennett GL (2012) Space applications. In: Rowe DM (ed) Handbook of thermoelectrics. CRC Taylor & Francis, Boca Raton, pp 515–535
2. Rowe WM (1991) Applications of nuclear-powered thermoelectric generators in space. Appl Energy 40(4):241
3. O'Brien RC, Ambrosi RM, Bannister NP, Howe SD, Atkinson HV (2008) Safe radioisotope thermoelectric generators and heat sources for space applications. J Nucl Mater 377(3):506
4. Bell LE (2009) Addressing the challenges of commercializing new thermoelectric materials. J Electron Mater 38(7):1344
5. Zhang QH, Huang XY, Bai SQ, Shi X, Uher CU, Chen LD (2016) Thermoelectric devices for power generation: recent progress and future challenges. Adv Eng Mater 18(2):194
6. Liu W, Jie Q, Kim HS, Ren Z (2015) Current progress and future challenges in thermoelectric power generation: from materials to devices. Acta Mater 87:357–376
7. LeBlanc S (2014) Thermoelectric generators: linking material properties and systems engineering for waste heat recovery applications. Sustain Mater Technol 1–2:26–35
8. Kim HS, Liu WS, Ren ZF (2017) The bridge between the materials and devices of thermoelectric power generators. Energ Environ Sci 10:69–85
9. Hendricks TJ, Crane DJ (2012) Thermoelectrics and its energy harvesting. In: Rowe DM (ed) Modules Systems and Applications in Thermoelectrics. CRC Taylor & Francis, Boca Raton, pp 22–27
10. Sarhadi A, Bjørk R, Pryds N (2015) Optimization of the mechanical and electrical performance of a thermoelectric module. J Electron Mater 44(11):4465
11. Karri NK, Mo C (2018) Reliable thermoelectric module design under opposing requirements from structural and thermoelectric considerations. J Electron Mater 47:3127
12. Hendricks TJ (2006) Thermal system interactions in optimizing advanced thermoelectric energy recovery systems. J. Energy Resour. Technol 129(3):223–231
13. Crane DT, Bell LE (2007) Design to maximize performance of a thermoelectric power generator with a dynamic thermal power source. ASME. Energy sustainability, ASME 2007 energy sustainability conference, pp 361–369. https://doi.org/10.1115/es2007-36210
14. Kumar S, Heister SD, Xu X, Salvador JR (2015) Optimization of thermoelectric components for automobile waste heat recovery systems. J Electron Mater 44(10):3627
15. Montecucco A, Siviter J, Knox AR (2015) Constant heat characterisation and geometrical optimization of thermoelectric generators. Appl Energy 149:248
16. Li Y, Yang XQ, Zhai PC, Zhang QJ (2008) Thermal stress simulation and optimum design of thermoelectric unicouples with graded interlayers. AIP Conf Proc 973:297–302
17. Clin T, Turenne S, Vasilevskiy D (2009) Numerical simulation of the thermomechanical behavior of extruded bismuth telluride alloy module. J Electron Mater 38:994
18. Turenne S, Clin T, Vasilevskiy D (2010) Finite element thermomechanical modeling of large area thermoelectric generators based on bismuth telluride alloys. J Electron Mater 39:1926
19. Al-Merbati AS, Yilbas BS, Sahin AZ (2014) A model study for cyclic thermal loading and thermal performance of a thermoelectric generator. Int J Energy Res 38:1351
20. Erturun U, Erermis K, Mossi K (2014) Effect of various leg geometries on thermo-mechanical and power generation performance of thermoelectric devices. Appl Therm Eng 73:128
21. Bakhtiaryfard L, Chen YS (2016) Design improvement of thermal elements in order to reduce thermal stresses in thermoelectric modules. Int J Appl Eng Res 11(17):9128
22. Fan S, Gao Y (2018) Numerical simulation on thermoelectric and mechanical performance of annular thermoelectric generator. Energy 150:38
23. Fan S, Gao Y (2019) Numerical Analysis on the segmented annular thermoelectric generator for waste heat recovery. Energy 183:35
24. Jia X, Gao Y (2014) Estimation of thermoelectric and mechanical performances of segmented thermoelectric generators under optimal operating conditions. Appl Therm Eng 73:335
25. Erturun U, Erermis K, Mossi K (2015) Influence of leg sizing and spacing on power generation and thermal stresses of thermoelectric devices. Appl Energy 159:19
26. Karri NK, Mo C (2018) Structural Reliability Evaluation of Thermoelectric Generator Modules - Influence of End Conditions, Leg Geometry, Metallization, and Processing Temperatures. J Electron Mater 47:6101
27. Kishore RA, Sanghadasa M, Priya S (2017) Optimization of segmented thermoelectric generator using Taguchi and ANOVA techniques. Scientific Reports 7:16746
28. ANSYS Release 15.0.0, ANSYS Inc, Canonsburg, PA
29. Angrist SW (1982) Direct Energy Conversion, 4th edn. Allyn and Bacon Inc, Boston, MA, p 145
30. Sherman B, Heikes RR, Ure Jr RW (1960) Calculation of efficiency of thermoelectric devices. J Appl Phys 31(1):1–16. https://doi.org/10.1063/1.1735380
31. Montgomery DC (2013) Design and analysis of experiments, 8th edn. Wiley, Hoboken
32. Myers RH, Montgomery DC, Anderson-cook CM (2009) Response surface methodology—process and product optimization using designed experiments, 3rd edn. Wiley, Hoboken
33. JMP®, Version 13.1.0. SAS Institute Inc., Cary, NC, 1989–2016
34. Derringer G, Suich R (1980) Simultaneous optimization of several response variables. J Qual Technol 12(4):214
35. Mean Absolute Error (2011) In: Sammut C, Webb GI (eds) Encyclopedia of machine learning. Springer, Boston
36. Fan M, Hu J, Cao R, Xiong K, Wei X (2017) Modeling and prediction of copper removal from aqueous solutions by nZVI/rGO magnetic nanocomposites using ANN-GA and ANN-PSO. Sci Rep 7(18040):1